

Self-assembled nanodot arrays on Si(111)-(7×7) surfaces

M. Yoon, X. F. Lin, I. Chizhov, H. Mai, and R. F. Willis*

Department of Physics, The Pennsylvania State University, University Park, Pennsylvania 16802

(Received 11 July 2000; revised manuscript received 1 November 2000; published 8 August 2001)

We report on the self-assembly of a superlattice of nanodots of different elements (Sn,In) on a Si(111)-(7×7) template surface, observed with a scanning tunneling microscope. The formation of nanodots is a feature of the Si(111)-(7×7) surface, and a characteristic of adsorbates of different valency. In this paper, we examine the evolution of these nanodots with increasing coverage to understand the clustering mechanism, their microstructure, and electronic properties. The results are discussed in the light of current theories of the interaction mechanism(s) guiding the formation of these nanodots.

DOI: 10.1103/PhysRevB.64.085321

PACS number(s): 68.37.Ef, 61.46.+w, 68.35.Bs, 68.35.Md

The self-assembled formation of ordered nanodots on solid surfaces with uniform and controllable size are of increasing interest as they offer unusual quantum properties and potential for devices in nanotechnology.^{1,2} The self-assembly of a superlattice of nanodots is a feature of the Si(111)-(7×7) surface, and a characteristic of adsorbates of the varying valency.^{3–6} Observations using scanning tunneling microscopy (STM)^{7–11} [shows a clustering of atoms within each 7×7 unit cell, which is preserved during room-temperature adsorption. Based on density-functional theory DFT total energy calculations, Cho and Kaxiras^{4,5} have proposed that the individual atoms collect within “basins of electrostatic potential” surrounding specific high-coordination number lattice sites, shown schematically, Fig. 1. The metallicity of the surface is preserved, and the individual potential wells are produced by charge redistribution between restatom and adatom states straddling the Fermi energy. Experimental evidence for this phenomena has been reported for the case of thallium adsorption.⁷ Up to 0.2 monolayer (ML) coverage, the Tl atoms cluster together to form nanodots while maintaining metallic electronic properties at the surface. There are three potential wells around rest atom sites in each half-cell,^{4,5} which are unresolved, the STM images showing triangular-shaped nanodots confined, preferentially, to the faulted-half (*F*) of the Si(111)-(7×7) unit cell, Fig. 2. This preference for the *F* half-cell over the unfaulted (*U*) half-cell is also predicted by the theory.⁶

This mechanism^{4,5} is independent of the valence of the adsorbate, providing the surface template structure and metallic behavior is not disturbed. However, there exists a tendency for the adatoms to bond with the surface dangling bonds of the silicon.³ When this happens, and dependent on the electronegativity of the adsorbate atoms,³ dangling bond states at the Fermi energy are removed and the surface becomes nonmetallic.^{8,9,12} The preference for adsorption on the *F*-half over the *U*-half unit cell is no longer so obvious but, nevertheless, the 7×7 lattice is preserved, and an ordered array of nanodots occurs.

In this paper, we look in detail at nanodot formation on Si(111)-(7×7) by monitoring the evolution of these nanostructures with increasing adsorbate coverage with STM. We choose to contrast the behavior of Sn, a group IV_A element and In, a group III_A element, in order to make a comparison with the reported results for Tl (group III_A)⁷ and Pb (Group IV_A).^{6,8}

We observe nanodot formation in all of these instances. However, in the case of the Sn, In, and Pb, the surface becomes nonmetallic.^{8,12} We report detailed structures of the evolution of the Sn nanodot structures. The reduced screening permits more fine structure to be resolved in the STM than has hitherto been the case. This allows us to model the growth of the nanodots and establish their shape. The nanodots occupy both halves of the 7×7 unit cell and produce a two-dimensional (2D) superlattice array on top of the Si(111)-(7×7) substrate lattice, which is preserved. Using scanning tunneling spectroscopy (STS), a gap opens up about the Fermi surface, the size of which indicates strong adsorbate-substrate bonding. Once formed (~0.5 ML) this 2D array of nanodots remains stable to further adsorption, with atoms condensing into metallic islands on this 2D array.

The experiments were performed in an ultrahigh vacuum (UHV) chamber with a base pressure of 2×10^{-10} Torr. The *n*-type Si sample was cleaned using acetone, methanol, pure alcohol, and annealed in UHV until a well-defined 7×7 low-energy electron diffraction (LEED) pattern was obtained.

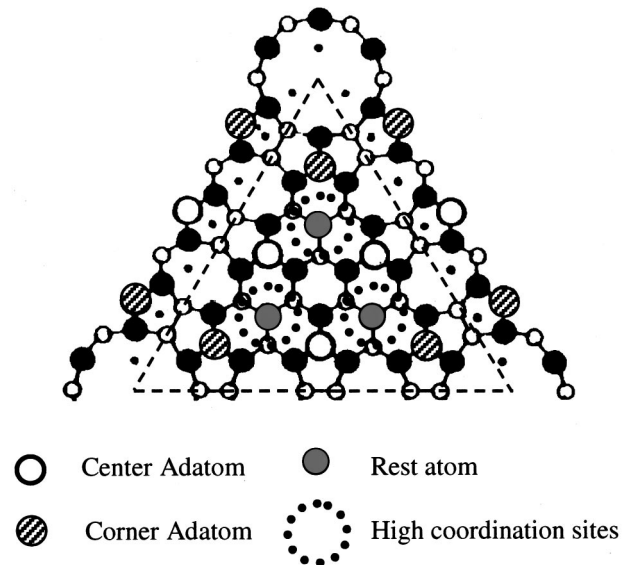


FIG. 1. Dimer-adatom-stacking-fault (DAS) model of the Si(111)-(7×7) unit cell proposed by Takayanagi *et al.* Corner and center adatoms, rest atom, and the high-coordination sites are shown.

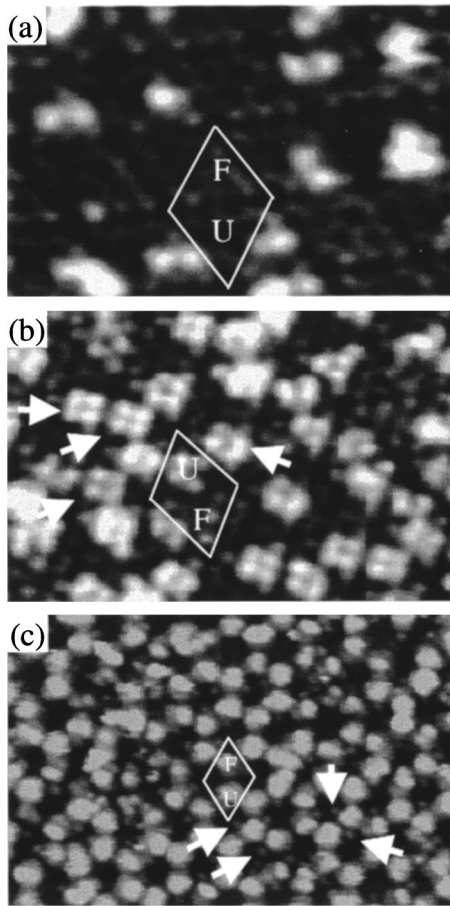


FIG. 2. Sequence of STM topographic images showing Sn on Si(111) obtained at (a) $\Theta \sim 0.03$ ML ($\sim 130 \times 80 \text{ \AA}^2$; $V_s = -2.1$ V, $I = 1$ nA); (b) $\Theta \sim 0.1$ ML ($\sim 170 \times 110 \text{ \AA}^2$; $V_s = -2.4$ V, $I = 1.4$ nA); (c) $\Theta \sim 0.3$ ML ($\sim 240 \times 155 \text{ \AA}^2$; $V_s = -2.2$ V, $I = 1$ nA). The faulted and unfaulted halves are labeled *F* and *U*, respectively. Some of tetramers, uncovered corner adatoms in sub-unit cell are marked by filled arrows in (b) and (c), respectively.

Keeping the sample at room temperature, Sn and In were resistively evaporated from an evaporator. The metal flux was monitored by a crystal thickness monitor. The Si(111)-(7 \times 7) surface structure was confirmed by STM and LEED before dosing and all STM images were taken at room temperature.

Figure 2 shows a sequence of STM topographic images recording the evolution of the superlattice array of Sn nanodots. The images were recorded with a negative sample bias voltage, reflecting a spatial distribution of occupied surface electronic states. The filled-state(s) image, Fig. 2(a), shows bright spots within each 7 \times 7 unit cell corresponding to tunneling out of (primarily) adatom states.¹² The bias voltage was -2.1 V and the tunneling current was 1 nA. Under these conditions, the *F*-half of the diamond-shaped 7 \times 7 unit cell appears brighter overall than the *U*-half. These two triangular-shaped half-cells are delineated by dark areas associated with Si dimers and corner holes.^{13–15} At a coverage of 0.03 ML, the ratio of the Sn atoms adsorbed on the *F*- and *U*-halves is approximately 2.3. A STS study of this low coverage surface, Fig. 2(a), suggests a strong covalentlike inter-

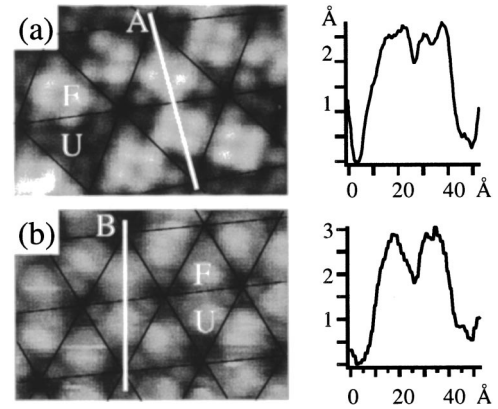


FIG. 3. (a) STM image of Sn on Si(111) at $\Theta \sim 0.1$ ML. Line scan along A in image is shown. (b) STM image of Sn on Si(111) at $\Theta \sim 0.3$ ML. Line scan along B in image is presented.

action between the Sn atoms and the dangling-bond surface states.¹² The Sn atoms interact with and remove dangling bond states at the Fermi level, opening up an energy gap, and a metal–insulator transition occurs in the Si(111)-(7 \times 7) surface electronic behavior. A preferential adsorption of adatoms on the *F*-halves of Si(111)-(7 \times 7) unit cell, at low coverages, has been widely reported for a large variety of metallic elements^{9–12,16} and confirmed by DFT calculations.³

As the Sn coverage increases to 0.1 ML [Fig. 2(b)], the tendency of the Sn atoms to form clusters becomes apparent in both *F*- and *U*-half cells. The statistical population ratio of Sn atoms adsorbed on *F*- and *U*-half cells falls from 2.3 to about 1.5, which suggests a decrease in the energy barrier separating the *F*- and *U*-half cells.^{6,7} “Atomic” structure is resolved within the nanostructures, suggesting nonmetallic, localized charge density. Comparing images in Figs. 2(a) and 2(b), we note that the nanodots have evolved from dimers and trimers [Fig. 2(a) discussed in Ref. 12] to mainly tetramers [Fig. 2(b)]. Increasing the Sn coverage still further to 0.3 ML [Fig. 2(c)], produces a quasicrystalline array of nanodots, occupying both halves of the Si(111)-(7 \times 7) unit cell and reflecting the overall hexagonal symmetry of the surface 7 \times 7 template underneath. At this coverage, “atomic features” within individual nanodots are no longer resolved. This is not due to a lack of tip resolution, as seen by comparison of Figs. 2(b) and 2(c). Atomic features are no longer as clearly resolved due to a change in the electronic properties/microstructures of the nanodots. The charge density appears to be more delocalized.

A closer look at the composition of the nanodots and their registry with the 7 \times 7 sublattice is shown in Fig. 3. Figure 3(a) shows the nanodots at 0.1 ML coverage [cf. Fig. 2(b)]. Figure 3(b) is a similar STM image showing nanodots formed at 0.3 ML coverage [cf. Fig. 2(c)]. It is apparent that the Sn nanodots are not randomly distributed within the sub-unit half-cells, but occupy specific sublattice sites. Line profiles taken along the line A across the unit cell in Fig. 3(a), gives an indication of the evolving size of the nanodots. The line profile A in Fig. 3(a) shows a topographical heights difference ($\sim 2.5 \text{ \AA}$) of the nanodots relative to that across a

corner hole of the Si(111)-(7×7) unit cell. The careful investigation of these clusters suggests that they mainly occupy the center of a subunit cell on Si(111)-(7×7). This experimental evidence implies that the first step of Sn atom condensation on Si(111)-(7×7) is the adsorption of single atoms on the dangling bonds of rest atoms and center adatoms. Initial adsorption on adatom sites induces reverse charge transfer from the Si rest atoms back to the Si adatoms, such that the rest atoms energetically now have an equal probability to bond with Sn, although they are in a different surface layer. A subtle change in the nature of these clusters occurs around 0.3 ML coverage, Fig. 3(b). This is apparent from the contrast in the images, Fig. 3. Also as we can see from the line profiles in Fig. 3, the clusters at 0.3 ML coverage, show a more pronounced dip between the *F* and *U* half-cells and more pronounced peaks (~3 Å) at 15 and 35 Å. We interpret the 0.5 Å height increase as being due to the adsorption of an extra Sn atom above a ring of adsorbed atoms. From the STM images, Fig. 3, we can observe two effects: the adsorption occurring on adatom and rest atom sites randomly, and the condensation of adsorbate atoms on top of adsorbed atoms. These results show interactions between Sn adsorbate atoms occurring at higher adsorbate coverage. Also, diffusion over the potential barrier between *F*- and *U*-halves is distinctively decreased while the Sn adsorbates become less mobile as the coverage is increased. Sonnet *et al.*⁶ have presented a theoretical study of the adsorption and the diffusion mechanisms of Pb on the Si(111)-(7×7) surface by using the empirical crystalline extension of the extended Hückel theory. Based on these studies, the authors have proposed that there are two adsorption mechanisms: the adsorption of Pb atoms on Si dangling bonds and Pb adsorption with formation of Pb atom clusters. They found that although the two mechanisms maybe coexist during the adsorption process, the formation of Pb atom clusters is favored due to a strong interaction between Pb atoms. However, there are significant differences between Pb and Sn despite their both being group IV_A elements. Unlike Pb on Si(111)-(7×7),⁶ Si corner adatoms sites are not preferential adsorption sites for Sn adsorption, as we can see in Fig. 2(b) and is indicated by an arrow in Fig. 2(c) for uncovered corner adatoms. This experimental evidence cannot be explained by the model by Cho and Kaxiras.⁵ First, the adsorption of a cluster of atoms at the high-coordination sites, Fig. 1, would prevent the corner adatoms being imaged in the STM, Fig. 2.⁴ Second, clustering of atoms about these high-coordination sites would not produce the line profile *B*, shown in Fig. 3(b). Incidentally, a similar line profile to Fig. 3(b) is observed for Tl/Si(111)-(7×7).^{4,5,7} Also, in the case of Pb atoms, which have a size comparable to Tl, the behavior is different again in that there is a surface reconstruction, destroying the metallicity of the Si(111)-(7×7) lattice while retaining a 7×7 symmetry.

The constant current topographic STM image, Fig. 4(a), shows a self-assembled array of nanodots of Sn atoms deposited at room temperature (0.5 ML coverage) onto a Si(111)-(7×7) surface template. The surface is nonmetallic, as is seen by the energy gap between states on either side of the Fermi energy [Fig. 4(b)], revealed by STS. The Sn

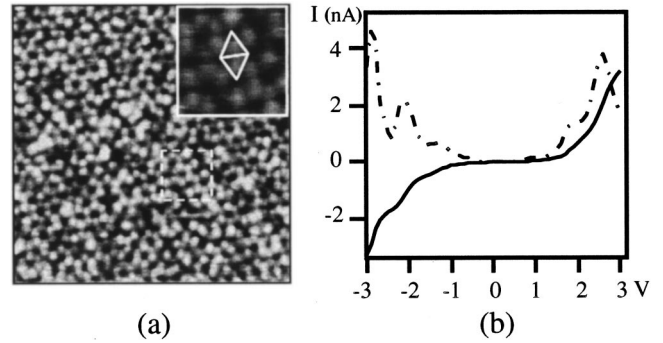


FIG. 4. Constant-current topographic STM image of Si(111)-(7×7) covered with ~0.5 ML of Sn at room temperature. (a) ~500×500 Å², ($V_s = -2.3$ V, $I = 1.5$ nA); (b) STS spectrum from the Sn clusters shows the *I-V* curve (solid line) and differential *I-V* curves (dash-dotted lines). The inset shows the magnified STM image of the area noted by a small rectangle in (a).

nanodots, Fig. 4(a), occupy both the *F* and *U* triangular-shaped half-cells of the 7×7 lattice, bounded by walls of Si dimers and corner holes, which remains uncovered. This suggests a significant energy barrier containing the nanodots, as was reported for thallium.⁷ The Sn case is different in that adsorption occurs in both half-cells suggesting that any energy barrier to diffusion between *F*- and *U*-halves of the 7×7 unit cell is lower than is the case with thallium. That such an energy barrier exists, however, is evidenced by a preference for initial adsorption within the *F* half-cell at lower coverages, as discussed in Ref. 12.

We have also studied the evolution of the surface morphology as a function of coverage for room temperature (RT) deposition using LEED. In Fig. 5(a) we show a LEED pattern for a clean Si(111)-(7×7) surface. Deposition onto this Si(111)-(7×7) surface at RT, reveals 1/7 order diffraction beams from the Si substrate decreasing in their intensity. Figures 5(b) and 5(c) shows LEED patterns evolving with Sn coverages of 0.5 and 3 ML, respectively. Below 0.5 ML, the LEED pattern remains relatively unchanged, with some increase in background scattering with decreased overall intensity, Fig. 5(b). Above 3 ML, Fig. 5(c), the 1/7 order spots have almost disappeared. No diffraction pattern from the Sn deposit itself was observed until 3 ML. There was no evidence of epitaxial growth of gray Sn semiconducting layers on Si(111)-(7×7) substrates at these coverages, which accords with previous LEED observations.^{17,18}

Figure 6(a) shows three-dimensional (3D) condensate droplets of Sn growing on top of the predeposited nanodot array at 1.0 ML coverage. The height of the large particle imaged in Fig. 6(a) is ~40 Å. We interpret this feature to be due to a free diffusion of additional Sn atoms on top of the 2D array of nanodots and eventual nucleation into larger size particles. Continued deposition up to 3.0 ML coverage creates a distorted coalescence of such particles, Fig. 6(b). The experimental evidence suggests that a uniform layer of 2D Sn nanodots first covers the whole surface before 3D islands form with further deposition.¹⁹

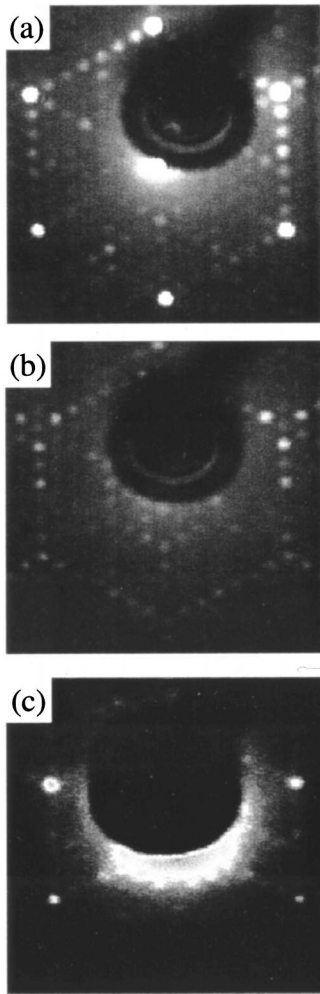


FIG. 5. LEED patterns at 44 eV from Sn on a Si(111)-(7x7) surface deposited at room temperature. (a) Clean Si(111)-(7x7) surface. (b) ~0.5 ML Sn coverage. (c) ~3 ML Sn coverage. The intensity and contrast were increased in (c) for better display.

Based on this experimental evidence, Fig. 7 shows a possible model of the formation of these self-assembled Sn nanodots. Figure 7(a) shows the preferential sites for initial adsorption, based on the experimental result, Fig. 3(a), which produces a ringlike aggregation composed of six Sn atoms. Similar ringlike nanostructures have been reported experimentally for Ag on Si(111)-(7x7)⁹ and are consistent with theoretical studies of adsorption at preferred bonding sites

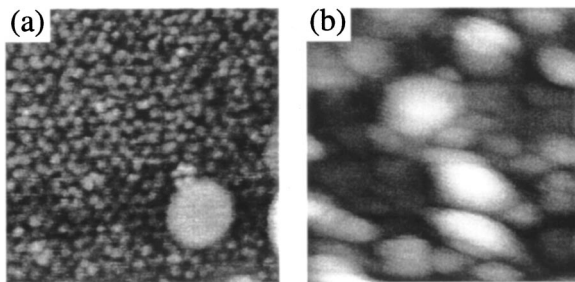


FIG. 6. (a),(b) 3D Sn islands growing on the predeposited 2D Sn overlayer at $\Theta \sim 1$ and ~ 3 ML, respectively.

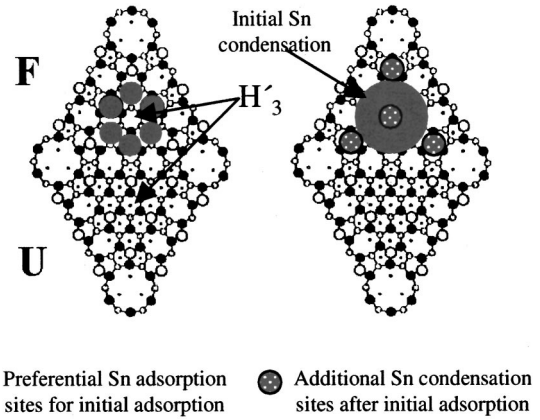


FIG. 7. Top view of the DAS model for the Si(111)-(7x7) reconstruction with proposed model for nanodot formation of Sn. (a) Preferential Sn adsorption sites due to initial condensation of adsorbate atoms. (b) Additional Sn condensation sites after initial adsorption.

for Pb on Si(111)-(7x7) surface.⁶

Figure 7(b) shows a further aggregation in size with increasing coverage up to 0.5 ML based on STM images [Figs. 2(c) and 4(a)] and analysis of the line profiles across these nanodots [Fig. 3(b)]. Sn atoms now adsorb on corner adatom sites and condense at the center of the ringlike nanostructures. Unlike the case of thallium nanodots,⁷ we see no evidence for migration of individual atoms or dots between the two half-cells. The Sn nanodot array remains quite stable against additional Sn adsorption.

The constant current topographic STM image, Figs. 8(a) and 8(b) shows a STM image and STS, respectively, of a self-assembled array of nanodots of In (Group III) atoms deposited at room temperature (0.5 ML coverage) onto a Si(111)-(7x7) surface template. The In nanodots [arrow A in Fig. 8(a)] occupy both the faulted (F) and unfaulted (U) triangular-shaped half-cells of the 7x7 lattice, bounded by walls of Si dimers and corner holes [arrow B in Fig. 8(a)] which remains uncovered. This is in stark contrast to the behavior reported for thallium (Group III),⁷ where clustering

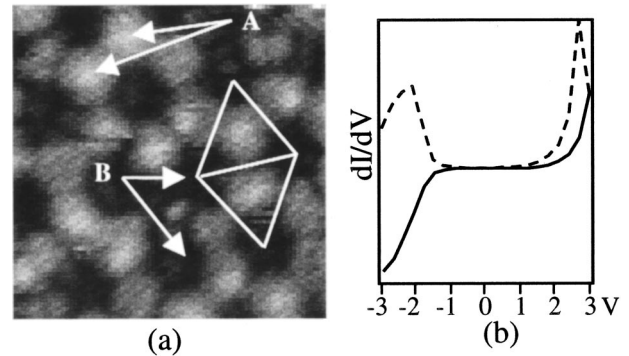


FIG. 8. Constant-current topographic STM image of Si(111)-(7x7) covered with ~0.5 ML of In at room temperature. (a) $\sim 85 \times 85 \text{ \AA}^2$, ($V_s = -2.2 \text{ V}$, $I = 1.5 \text{ nA}$); (b) STS spectrum from the In clusters shows the $I-V$ curve (solid line) and differential $I-V$ curves (dashed lines).

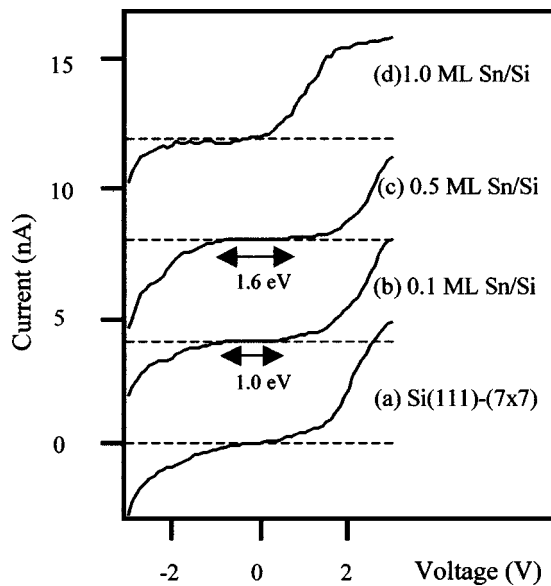


FIG. 9. Current-vs-voltage measurement over various Sn coverage on room temperature Sn/Si(111). Curve (a), region of clean Si(111)-(7 \times 7); curve (b), region of Sn adsorbate atoms at \sim 0.1 ML [from Fig. 2(b)]; curve (c), region of 2D Sn cluster at \sim 0.5 ML [from Fig. 4(a)]; curve (d), region of 3D Sn island [from Fig. 6(a)].

occurs within the F -half-cells exclusively and the surface remains metallic. This experimental evidence suggests that the mechanism of self-assembled nanodots for Sn and In is very similar but very different to Tl.

Figure 9 shows I - V curves changing with coverage of Sn atoms. The Si(111)-(7 \times 7) clean surface is initially metallic [Fig. 9(a)], with a small but finite slope of the I - V curve as the bias voltage is swept through zero.²⁰ Depositing 0.1 ML of Sn atoms opens a gap of 1.0 eV due to the removal of

adatom states about the Fermi energy, Fig. 9(b). Detailed $d \ln I/d \ln V$ spectroscopy¹² suggests bonding of Sn atoms primarily to adatom dangling bonds. At 0.5 ML, the surface consists of a 2D array of Sn nanodots and the surface band-gap has increased to 1.6 eV, Fig. 9(c). These I - V measurements were obtained with the feedback loop stabilized around ± 2.0 V. The vertical scale is the tunneling current for the clean Si(111)-(7 \times 7) surface, the I - V curves for the different Sn coverages displaced vertically for clarity. Positioning the STM tip above a Sn condensate particle at 1.0 ML coverage, Fig. 9(d) shows a return to metallic behavior. This suggests that the nanodot interfacial sublattice is destroyed under these condensate particles and the Si(111)-(7 \times 7) sublattice recovers its metallicity.

In summary, we have presented evidence for a quite different mechanism for the formation of a superlattice of Sn nanodots on a Si(111)-(7 \times 7) template surface compared with that reported for thallium.⁷ As argued in the case of Sn, Tl, In, and Pb, these epitaxial layers are metastable phases due to the template nature of the Si(111)-(7 \times 7) substrate lattice. What is amazing is that, in all cases, the 7 \times 7 lattice retains its template nature, despite the very different adsorption and bonding characteristics of these elements. The tendency towards clustering and nanodot formation is a widespread tendency on this surface with a variety of different elements. However, whereas Tl appears to preserve the metallicity of the surface, most other elements, including Sn, In, Pb reported here, do not, despite preserving the 7 \times 7 sublattice. This suggests subtle differences in adsorbate-substrate interaction while preserving the diffusion barriers confining atoms to the individual 7 \times 7 half-cells.

Partial funding for this work was provided by a grant from the Office of Naval Research, ONR Grant No. N00014-92-J-1479.

*Correspondence should be sent to rfw4@psu.edu

¹H. Brune, M. Giovannini, K. Bromann, and K. Kern, *Nature (London)* **394**, 451 (1998).

²I. B. Altfeder, K. A. Matveev, and D. M. Chen, *Phys. Rev. Lett.* **78**, 2815 (1997).

³K. D. Brommer, M. Galván, A. Dal Pino, and J. D. Joannopoulos, *Surf. Sci.* **314**, 57 (1994).

⁴K. Cho and E. Kaxiras, *Europhys. Lett.* **39**, 287 (1997).

⁵K. Cho and E. Kaxiras, *Surf. Sci.* **396**, L261 (1998).

⁶Ph. Sonnet, L. Stauffer, and C. Minot, *Surf. Sci.* **407**, 121 (1998).

⁷L. Vitali, M. G. Ramsey, and F. P. Nezer, *Phys. Rev. Lett.* **83**, 316 (1999).

⁸E. Ganz, I. Hwang, F. Xiong, S. Theiss, and J. Colovchenko, *Surf. Sci.* **257**, 259 (1991).

⁹St. Tosch and H. Neddermeyer, *Phys. Rev. Lett.* **61**, 349 (1988).

¹⁰U. K. Köhler, J. E. Demuth, and R. J. Hamers, *Phys. Rev. Lett.* **60**, 2499 (1988).

¹¹A. Watanabe, M. Naitoh, and S. Nishigaki, *Jpn. J. Appl. Phys., Part 1* **37**, 3778 (1998).

¹²X. F. Lin, I. Chizhov, H. A. Mai, and R. F. Willis, *Surf. Sci.* **366**, 51 (1996).

¹³K. Takayanagi, Y. Tanishiro, M. Takahashi, and S. Takahashi, *J. Vac. Sci. Technol. A* **3**, 1502 (1985).

¹⁴R. S. Becker, J. A. Golovchenko, D. R. Hamann, and B. S. Swartzentruber, *Phys. Rev. Lett.* **55**, 2032 (1985).

¹⁵O. Nishikawa, M. Tomitori, F. Iwawaki, and N. Hirano, *J. Vac. Sci. Technol. A* **8**, 421 (1990).

¹⁶T. Hashizume, Y. Hasegawa, I. Sumita, H. Tanaka, S. Amano, S. Hyodo, and T. Sakurai, *J. Vac. Sci. Technol. B* **9**, 745 (1991).

¹⁷P. J. Estrup and J. Morrison, *Surf. Sci.* **2**, 465 (1984).

¹⁸T. Ichikawa, *Surf. Sci.* **140**, 37 (1984).

¹⁹M. Zinke-Allmany, H. J. Gossmann, L. C. Feldman, and G. J. Fisanick, in *Superlattices and Thin Films*, edited by J. D. Dow and J. K. Schuller, MRS Symposia Proceedings No. 77 (Materials Research Society, Pittsburgh, 1987), p. 703.

²⁰R. S. Becker, J. A. Golovchenko, D. R. Hamann, and B. S. Swartzentruber, *Phys. Rev. Lett.* **55**, 2032 (1985).